2010

Hot electron effects on efficiency degradation in InGaN light emitting diodes and designs to mitigate them

X. Ni
Virginia Commonwealth University

X. Li
Virginia Commonwealth University

J. Lee
Virginia Commonwealth University

See next page for additional authors

Ni, X., Li, X., & Lee, J., et al. Hot electron effects on efficiency degradation in InGaN light emitting diodes and designs to mitigate them. Journal of Applied Physics, 108, 033112 (2010). Copyright © 2010 American Institute of Physics.

Hot electron effects on efficiency degradation in InGaN light emitting diodes and designs to mitigate them

X. Ni,[1] X. Li,[1] J. Lee,[1] S. Liu,[1] V. Avrutin,[1] Ü. Özgür,[1] H. Morkoç,[1,a)] and A. Matulionis[2]
[1]*Department of Electrical and Computer Engineering, Virginia Commonwealth University, Richmond, Virginia 23284, USA*
[2]*Semiconductor Physics Institute, Center for Physical Sciences and Technology, A. Goštauto 11, 01108 Vilnius, Lithuania*

(Received 31 May 2010; accepted 6 June 2010; published online 10 August 2010)

Hot electrons and the associated ballistic and quasiballistic transport, heretofore neglected endemically, across the active regions of InGaN light emitting diodes (LEDs) have been incorporated into a first order simple model which explains the experimental observations of electron spillover and the efficiency degradation at high injection levels. The model is in good agreement with experiments wherein an adjustable barrier hot electron stopper, commonly called the electron blocking layer (EBL), is incorporated. The model is also in agreement with experiments wherein the electrons are cooled, eliminating hot electrons, inside a staircase electron injector (SEI) prior to their injection into the active region. Thermionic emission from the active region, even if one uses an uncharacteristically high junction temperature of 1000 K, fails to account for the carrier spillover and the experimental observations in our laboratory in samples with varying EBL barrier heights. The model has been successfully applied to both *m*-plane (lacking polarization induced electric field) and *c*-plane (with polarization induced field) InGaN double heterostructure (DH) LEDs with a 6 nm active region featuring a variable barrier hot electron stopper, and a SEI, and the various combinations thereof. The choice of DH LEDs stems from our desire to keep the sample structure simple as well as the model calculations. In this paper, the theoretical and experimental data along with their comparison followed by an insightful discussion are given. The model and the approaches to eliminate carrier spillover proposed here for InGaN LEDs are also applicable to GaN-based laser diodes. © *2010 American Institute of Physics*.
[doi:10.1063/1.3460271]

I. INTRODUCTION

The performance of InGaN-based light emitting diodes (LEDs) has improved considerably over the past few decades, and they are now penetrating the outdoor general lighting applications, and are poised to penetrate the indoor lighting applications as well. However, one critical issue for the application of the InGaN LEDs for general lighting is the lack of retention of the electroluminescence (EL) efficiency at high injection currents.[1] The external quantum efficiency (EQE) of InGaN LEDs has been observed to reach its peak value at relatively small current densities, below 50 A cm^{-2} in some cases, which bodes well for LEDs, but then decreases monotonically even under a low duty cycle short pulsed current, which does not bode well.[2] The physical origin of this EL efficiency loss at high currents in InGaN LEDs is heretofore not clearly understood and controversial, and thus the topic is open to further investigations. Carrier loss through nonradiative Auger recombination at high injection currents has initially been proposed for the efficiency degradation.[3–5] The Auger recombination coefficient deduced from a rate equation fit to the experimental photoluminescence (PL) data in an earlier effort is $1.4–2.0 \times 10^{-30}$ cm^6/s for quasibulk InGaN layers.[3] However, the value deduced from the third order polynomial fit varies several orders of magnitude among different reports. It should also be noted that this approach assumes the coefficients representing the nonradiative and radiative recombination processes to be injection independent which does not necessarily hold. Moreover, it has been established that the direct Auger recombination coefficient decreases exponentially with the band-gap energy.[6] This is backed by a more recent calculation using a fully microscopic many body model,[7] which shows that the Auger recombination involving only the lowest conduction band and the highest valence band is negligible when compared to the radiative recombination. This suggests that the carrier losses due to the Auger effect in InGaN based LEDs, particularly in those emitting at energies away from 2.5 eV,[5] would not necessarily be dominant. Moreover, when the efficiency loss at high injection currents is ascribed to Auger recombination alone through a standard third order polynomial rate equation fit of the EL efficiency among commercial LEDs, one arrives at unreasonably large Auger coefficients,[8] in the range of $10^{-27}–10^{-24}$ $cm^6\ s^{-1}$. These figures are at least three orders of magnitude higher than the other reported values,[3,5,9,10] which would imply that the Auger recombination alone (if at all) cannot be assumed to account for the degradation of EL efficiency in the InGaN LEDs.

Also inconsistent with the Auger recombination premise are the below-the-barrier resonant photoexcitation experiments (photons absorbed only in InGaN active region with

a)Electronic mail: hmorkoc@vcu.edu.

ensuing generation of *equal* number of cool electrons and holes followed by either radiative or nonradiative recombination only in the same region) where the efficiency degradation has not been noted at photocarrier generation rates comparable to, if not beyond, the electrical injection levels where the EL efficiency degrades.[11,12] This would then suggest that the EL efficiency degradation to a first extent is of electrical nature and that it is very likely to be related to the carrier injection, transport, and leakage processes.

The above discussion naturally leads to the conclusion that electron overflow is the dominant mechanism governing the efficiency loss at high current levels. It has been observed that in both polar *c*-plane, possessing internal polarization induced field, and nonpolar *m*-plane LEDs, featuring no such internal polarization induced field, the electron overflow (or spillover) results in a substantial EL efficiency reduction (by 70%–80%) when an electron blocking layer (EBL) is not employed.[13] In InGaN LEDs, while not the entire reason at this juncture, relatively low hole injection (due to relatively low hole concentration of p-GaN) and/or poor hole transport inside the active region (due to large hole effective mass) could exacerbate the electron overflow issue, as electrons need accompanying holes in the active region for recombination.[12,14] Theoretical calculations also indicate that electron concentration in equilibrium with the lattice even well above the room temperature would not have a sufficient Boltzmann tail to surpass the barrier for notable carrier spillover.[15]

The above-mentioned observations necessarily imply that nonequilibrium processes must be considered to account for the electron overflow process. In this regard, the present paper treats the ballistic and quasiballistic electron transport across the InGaN active region as a substantial source for the electron overflow and the associated EL efficiency loss. Basically, upon injection from the n-GaN layer into the InGaN active region the electrons gain additional kinetic energy equal to the conduction band offset between n-GaN and InGaN, in addition to the accelerating effect of any electric field present. These hot electrons have a short transit time and high probability to traverse the active region without thermalizing. They escape the radiative recombination in the active region and contribute to the overflow electron current. It should be noted that the concept of nonequilibrium hot electrons in the context of light emitters is nonconventional and represents a major deviation from the proverbial treatment of such devices. One can then surmise that models, particularly the commercially available software packages used to model the LEDs under discussion, which are void of the treatment of hot electrons, would be missing the major driving force for electron overflow. Moreover, we demonstrate that an InGaN staircase electron injector (SEI), with a step-like increased In composition, reduces if not fully eliminate the ballistic and quasiballistic electron overflow, the particulars being dependent on the active region design and the electric field present therein. The SEI structure serves to cool the electrons and bring them to equilibrium with the lattice in the active region where their radiative recombination with holes takes place if the holes are present.

In this paper, we will first formulate the electron overflow due to the hot electrons and also show the efficacyof a SEI for eliminating the hot electron-induced electron overflow. This is then followed by our experimental data for both *c*-plane and *m*-plane cases which support the nonequilibrium hot electron mitigated electron overflow argument. The paper will conclude with a discussion bringing together all the observations and in the process shedding the much needed light on such an important problem facing the LED lighting community.

II. THEORETICAL APPROACH FOR ELECTRON OVERFLOW

A. Electron overflow due to thermionic emission

At the onset with no *a priori*-inclination, we need to consider that the electron overflow might have its origin in two possible phenomena: (*i*) thermionic emission of equilibrium electrons from the bottom of the active region over the barrier into the p-layer (we will show this not to be important due to large band discontinuity for our investigated LEDs), (*ii*) ballistic and quasiballistic transport of the injected electrons that do not thermalize while in the active region. Let us consider the former point through numerical simulations using the SILVACO ATLAS software for a p-GaN/$In_{0.20}Ga_{0.80}N$/n-GaN LED without an EBL. For the calculations, the electrons were assumed to be completely thermalized and in equilibrium in the active region. For this and also the rest of the calculations, the commonly accepted material parameters were used for the $In_{0.20}Ga_{0.80}N$ active layer; a Shockley–Read–Hall (SRH) recombination coefficient (A) of 1×10^{7} s^{-1}, a spontaneous radiative recombination coefficient (B) of 1×10^{-11} cm^{3} s^{-1}, and an Auger recombination coefficient (C) of 1×10^{-30} cm^{6} s^{-1} were assumed. For p-GaN, an A coefficient of 1×10^{10} s^{-1} (corresponding to a lifetime of 100 ps) was used. The conduction band offset ΔE_c between $In_{0.20}Ga_{0.80}N$ and p-GaN was deduced to be 0.5 eV by assuming 70% of the total band gap discontinuity.

The simulations involving the above-mentioned thermionic emission show that even at an uncharacteristically elevated junction temperature of 1000 K and at an unreasonably high current density of 1×10^{4} A cm^{-2}, the thermionic emission driven overflow electron current into the p-GaN region is only ~11% of the total current density. At the same current density of 1×10^{4} A cm^{-2}, the corresponding values are ~1% and ~0% for junction temperatures of 700 K and 500 K, respectively. The calculated energy distributions of electrons for several junction temperatures are shown in Fig. 1, where they are compared on a flat band diagram for simplicity. Keeping in mind the large discrepancy for the Auger coefficient,[3–6] the calculated electron overflow values are 0%, 3%, and 36% for junction temperatures of 500 K, 700 K, and 1000 K, respectively, if an Auger coefficient of 1×10^{-34} cm^{6} s^{-1} is assumed. Notably, such a meager tail of the electron distribution within a thermal energy (kT) of and above the barrier on the p-side of the junction cannot account for the observed three to five times EL difference between the LEDs with and without EBL.[13] This indicates that the genesis of the notable electron overflow is not the thermionic

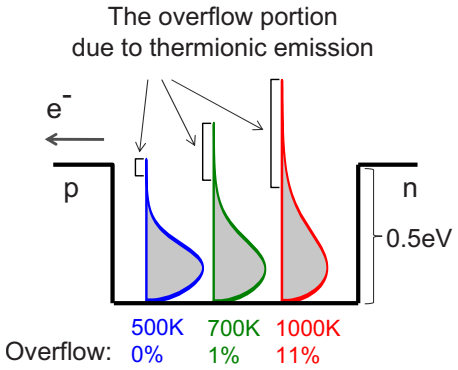

FIG. 1. (Color online) Calculated energy distribution of electrons in the active region at 3 different junction temperatures: 500, 700, and 1000 K. A flat band diagram schematic is used just to show the barrier height of the p-GaN and for a comparative picture of the three distributions, which actually correspond to three different band diagrams. The integrated tail of the Fermi–Dirac distribution makes up only 0%, ~1%, and ~11% of the total current at the junction temperatures of 500 K, 700 K, and 1000 K, respectively.

emission of the equilibrium electrons from the active region even in the LEDs without EBL. We must therefore turn our attention to nonequilibrium electrons, in other words hot electrons, inside the $In_{0.20}Ga_{0.80}N$ (the particular composition used in our experiments) active region. The injected hot electrons can traverse the active layer by ballistic or quasiballistic transport and recombine in the p-GaN region instead of the active region. We should note that the nonradiative recombination is prevalent in p-type GaN due to its defective nature, and any radiative recombination in the p-GaN would produce an unwanted wavelength in addition to that emanating from the designed active region.

B. Hot electron transport and ensuing overflow in InGaN LEDs

Having made the suggestion that the electron overflow current might be due to ballistic and quasiballistic transport of the injected electrons through the active region, we will in this section discuss a first order estimation of the hot electron effect and attempt to explain our data with varying barrier height of the EBL in this framework. The calculation assumes that the electrons obey the Fermi–Dirac distribution in the n-GaN layer, i.e., before they are injected into the active region. The electrons acquire the additional kinetic energy equal to the conduction band offset between n-GaN and $In_{0.20}Ga_{0.80}N$ ($\Delta E_c \sim 0.5$ eV in this case) upon injection. These hot electrons would either undergo thermalization and lose their excess energy mainly through interaction with LO phonons[16] or avoid thermalization and leave the InGaN region as depicted in Fig. 2.

Our calculations take into account the ballistic electrons, representing those that experience no scattering in the active region, and the quasiballistic electrons that experience one scattering event (i.e., quasiballistic motion involving either LO phonon emission or absorption), and two scattering events (four combinations of two scattering events involving LO phonon emission and absorption). As will be evident soon those experiencing multiple energy loosing scattering events are eventually thermalized. In the calculations the

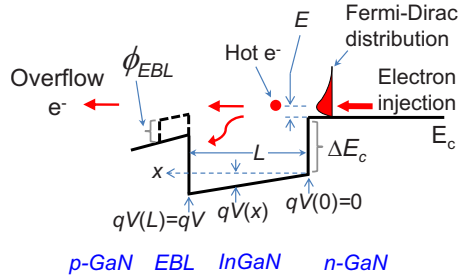

FIG. 2. (Color online) Schematic of electron overflow caused by ballistic or quasiballistic electron transport across the InGaN active region. The electrons gain a kinetic energy after being injected into InGaN, which equals to $E+\Delta E_c+qV(x)$. These hot electrons will either traverse the active region ballistically and quasiballistically, escape recombination inside InGaN, and contribute the electron overflow current, or be thermalized and captured inside the active region through interactions with LO phonons.

electrons are categorized according to their scattering events that they experience: no scattering, one scattering event (one LO phonon emission or one LO phonon absorption), etc. We should mention that the calculated contribution of electrons undergoing two scattering events to the overflow, as we will demonstrate below, is less than 1% of the total injected electrons and can be ignored for a 6 nm thick active region as in our experimental device structures. Because of the negligible contribution of the electrons undergoing two scattering events, and necessarily beyond, to the electron overflow, let us consider below only three cases: (*i*) no scattering, (*ii*) one phonon emission, and (*iii*) one phonon absorption.

1. Case 1. Truly ballistic case

As shown in Fig. 2, at position x inside the InGaN layer, the kinetic energy of an electron is $E+\Delta E_c+qV(x)$, where E is the excess energy in the n-GaN layer with respect to the conduction band of n-GaN, due to, e.g., band bending and kinetic/thermal energy (assuming electrons have a Fermi–Dirac distribution in n-GaN), ΔE_c is the conduction band offset between the InGaN and the n-GaN layers, $V(x)$ is the net potential drop within the active region at position x due to the electric field (including the effect of the built-in potential) with boundary conditions of $V(0)=0$ and $V(L)=V$, and L is the active region thickness. Therefore, the electron velocity at position x is $v(E+\Delta E_c+qV(x)) = \sqrt{2[E+\Delta E_c+qV(x)]/m_e}$, where m_e is the electron effective mass. The total time for the electron to traverse the active region is then $t=\int_0^L dx/v[E+\Delta E_c+qV(x)]$. The probability of the ballistic process is given by: $\exp(-t/\tau_{sc})$, where τ_{sc} is the phonon scattering time given by $\tau_{sc}=1/(1/\tau_{abs}+1/\tau_{em})$, where τ_{abs} and τ_{em} are the LO phonon absorption and emission times, respectively. We should mention that the phonon scattering time is actually dependent on the electron density and energy, but we will assume it to be constant in the present treatment for simplicity.[17] The percentage of the overflow electrons for *case 1*, which begin their journey in the n-GaN layer just prior to injection, is represented by the product of the probability of electrons having excess energy $E \geq \max\{0,(\phi_{EBL}-qV)\}$ above the conduction band in the n-GaN layer and the probability of ballistic electron transport across the active region

$$P_1 = \left[\int_{\max\{0,(\phi_{\mathrm{EBL}}-qV)\}}^{+\infty} f(E)N(E)\exp\left(\int_0^L \frac{-dx/\tau_{sc}}{v[E+\Delta E_c+qV(x)]} \right) dE \right] \Big/ \left(\int_0^{+\infty} f(E)N(E)dE \right), \tag{1}$$

where $f(E)$ is the Fermi–Dirac distribution function in the n-GaN, ϕ_{EBL} is the barrier height of the EBL (i.e., the conduction band offset between the EBL material and the p-GaN, which is 0 for the case with no EBL), and $N(E)$ is the conduction band density of states in the InGaN layer.

The calculation of Eq. (1) requires the potential distribution $V(x)$ inside InGaN layer, which requires numerical simulation packages such as SILVACO ATLAS. Due to the lack of inclusion of the hot electron models in the packages, the effect of potential inside the active region (i.e., the acceleration or deceleration by the electric field) on the electron velocity is neglected at the moment for *all cases* in the present work. In the *c*-plane LED case this would underestimate the electron overflow percentile as we will show in Sec. II D However, the barrier lowering at the p-region by the applied voltage across the active region has been taken into consideration in our model in order to account for the voltage dependent electron overflow. After neglecting the acceleration or deceleration of electrons by the electric field inside the active region, the exponential term in Eq. (1) could be simply replaced by $\exp[-L/v(E+\Delta E_c)/\tau_{sc}]$. For further simplicity, we assume that the electrons traverse only in the direction normal to the heterointerface, which would insignificantly overestimate the probability of escaping scattering events and overestimate the current overflow some.

2. Case 2. One phonon emission during electron transit across the active region

Let us start from the known electron distribution $f(E)$ in the n-GaN layer where the electrons are assumed to be in equilibrium with the lattice. Among the electrons, injected from the n-GaN layer, only those which still have enough energy to surmount the barrier at the p-side after one phonon emission inside the active region will contribute to the overflow current. The total probability of an electron overflowing to the p-side via one phonon emission (LO phonon energy $\hbar\omega_{\mathrm{LO}}=88$ meV) is the product of the following four partial probabilities:

(a) The probability of finding an electron in the n-GaN layer with an excess energy $E \geq (\phi_{\mathrm{EBL}}-qV+\hbar\omega_{\mathrm{LO}})$ above the bottom of the conduction band of the n-GaN before injection into the active region

$$P_a = \frac{\int_{\max\{0,(\phi_{\mathrm{EBL}}-qV+\hbar\omega_{\mathrm{LO}})\}}^{+\infty} f(E)N(E)dE}{\int_0^{+\infty} f(E)N(E)dE}. \tag{2}$$

(b) The probability to travel distance x from the n-GaN/InGaN heterointerface without being scattered

$$P_b = \exp(-[x/v(E+\Delta E_c)]/\tau_{sc}). \tag{3}$$

(c) The probability to emit an LO phonon between x and $x+dx$

$$P_c = [dx/v(E+\Delta E_c)]/\tau_{\mathrm{em}}. \tag{4}$$

(d) The probability to reach $x=L$, which is across the entire active region, without being scattered

$$P_d = \exp(-[(L-x)/v(E+\Delta E_c-\hbar\omega_{\mathrm{LO}})]/\tau_{sc}). \tag{5}$$

The overall probability or total percentile of the overflow electrons for one phonon emission, the *case 2*, is, therefore, given by

$$P_2 = P_a \cdot P_b \cdot P_c \cdot P_d = \int_{\max[0,(\phi_{\mathrm{EBL}}-qV+\hbar\omega_{\mathrm{LO}})]}^{+\infty} f(E)N(E) \int_0^L \frac{\exp\{-[x/v(E+\Delta E_c)]/\tau_{sc}\}}{v(E+\Delta E_c)\cdot\tau_{\mathrm{em}}} \times \exp\{-[(L-x)/v(E+\Delta E_c - \hbar\omega_{\mathrm{LO}})]/\tau_{sc}\} \cdot dx \cdot dE \Big/ \left[\int_0^{+\infty} f(E)N(E)dE \right]. \tag{6}$$

3. Case 3. One phonon absorption during electron transit across the active region

An approach similar to that of the *case 2* can be used, except for step (c) for which the phonon emission time is replaced with the phonon absorption time, noting that the velocity after one phonon absorption is $v(E+\Delta E_c+\hbar\omega_{\mathrm{LO}})$. Moreover, the integration in the numerator is performed from $E=\max\{0,(\phi_{\mathrm{EBL}}-qV-\hbar\omega_{\mathrm{LO}})\}$ to $+\infty$ to account for those electrons that are involved in this single phonon absorption process. The total percentage of the overflow electrons for the one phonon absorption process, *case 3*, is, therefore, given by

$$P_3 = \int_{\max[0,(\phi_{\mathrm{EBL}}-qV-\hbar\omega_{\mathrm{LO}})]}^{+\infty} f(E)N(E) \int_0^L \frac{\exp\{-[x/v(E+\Delta E_c)]/\tau_{sc}\}}{v(E+\Delta E_c)\cdot\tau_{\mathrm{abs}}} \times \exp\{-[(L-x)/v(E+\Delta E_c + \hbar\omega_{\mathrm{LO}})]/\tau_{sc}\} \cdot dx \cdot dE \Big/ \left[\int_0^{+\infty} f(E)N(E)dE \right]. \tag{7}$$

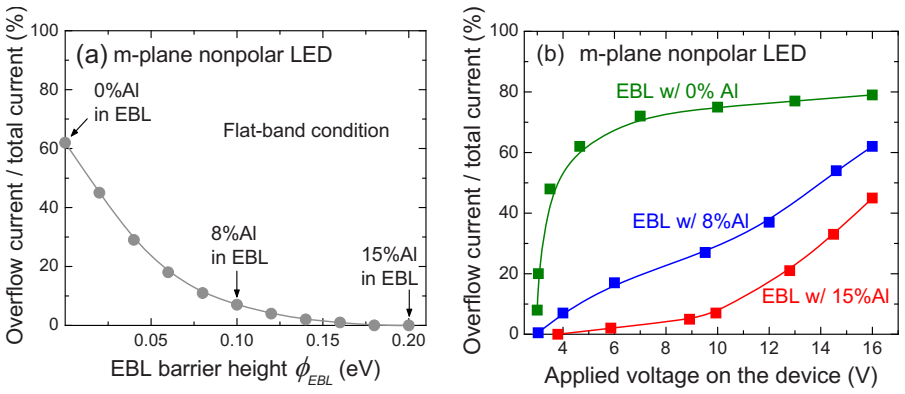

FIG. 3. (Color online) (a) Calculated ratio of the overflow electron current to the total current as a function of the EBL barrier height (ϕ_{EBL}) in nonpolar *m*-plane LEDs, assuming flat band conditions in the active region (i.e., 0 V net potential drop across the InGaN active region after the applied external voltage compensates the built-in potential, which is ~0.5 V), corresponding to 3.8, 4.0, and 4.7 V externally applied bias for the LEDs with 15%, 8%, and 0% Al in the EBL, respectively. (b) Calculated ratio of overflow electron current to the total current as a function of the applied voltage (forward direction) across the *m*-plane LEDs with three types of EBLs: 0% Al, 8% Al, and 15% Al. The symbols in (a) and (b) represent the calculated points whereas the lines are guides to the eye.

Another possible source of electron overflow is due to the electrons that undergo two scattering events: (i) one phonon absorption followed by one phonon emission, (ii) one phonon emission followed by one phonon absorption, (iii) two phonon emission, and (iv) two phonon absorption. For example, in a manner similar to that described above for single scattering events, the percentile of electron overflow for the case of "one phonon absorption followed by one phonon emission" can be written as

$$P_4 = \left[\int_0^{\infty} f(E)N(E)dE\right]^{-1} \int_{\max\{0,(\phi_{\mathrm{EBL}}-qV)\}}^{+\infty} f(E)\cdot N(E) \int_0^{L}\int_0^{x_2} \exp\{-[x_1/v(E+\Delta E_c)]/\tau_{sc}\}$$
$$\times \frac{\exp\{-[(x_2-x_1)/v(E+\Delta E_c+\hbar\omega_{\mathrm{LO}})+(L-x_2-x_1)/v(E+\Delta E_c)]/\tau_{sc}\}}{v(E+\Delta E_c)\cdot\tau_{\mathrm{abs}}\cdot v(E+\Delta E_c+\hbar\omega_{\mathrm{LO}})\cdot\tau_{\mathrm{em}}}\cdot dx_1\cdot dx_2\cdot dE. \quad (8)$$

Equation (8) takes into account the combined probabilities for an electron to reach the position x_1 without any scattering event, to absorb a phonon near x_1 $(0\leq x_1\leq x_2)$, reach the position x_2 without being scattered, emit a phonon near x_2 $(0\leq x_2\leq L)$, and finally escape the active region without being scattered between points x_2 and L. The integration over dx_1, dx_2, and dE accounts for all possible paths and all suitable electrons within the realm of processes discussed above. However, the contribution of these overflow electrons undergoing two scattering events is negligible and accounts for less than 1% of the total electron overflow.

Figure 3(a) shows the calculated percentile electron overflow (i.e., overflow electron current divided by the total current) as a function of ϕ_{EBL} for flat band conditions in an *m*-plane LED which is void of any polarization induced electric field. For all of the calculations, phonon emission (τ_{em}), absorption (τ_{abs}), and scattering times (τ_{sc}) of 0.01 ps, 0.1 ps, and 0.009 ps, respectively, have been used.[17] An LO phonon energy of $\hbar\omega_{\mathrm{LO}}=88$ meV has been used for InGaN layers.[18] To reiterate the aforementioned time constants are functions of the electron density, but in the present first order theory they will be assumed to be independent of electron density and energy. As mentioned, the calculated probabilities for the overflow by the electrons that undergo two or more scattering events are negligible (≤1%). Under the flat band conditions for the LED without EBL, meaning $y=0\%$ Al in $Al_yGa_{1-y}N$ EBL, a significant portion (~62%) of the total electron current is due to electrons escaping the active region altogether, while only 2% electron overflow occurs when an EBL with $y=15\%$ Al is inserted, as elaborated on below.

The calculated ratio of overflow electron current to the total current is shown in Fig. 3(b) as a function of the applied forward voltage (V_T) across the *m*-plane LEDs with different EBLs. The relationship between the internal voltage across the active region (V in the above equations) and V_T was obtained using SILVACO ATLAS with simulation parameters given in Sec. II A, neglecting the voltage drop across the metal/semiconductor contacts. The large applied biases resulting across the devices despite the fact that voltage drops across the contacts were neglected, point at the limitations of the simulation package, which however represents a suitable tool to show the trends in electron overflow. According to the numerical simulations by SILVACO ATLAS, the flat band conditions in the active regions are achieved at $V_T=3.8$, 4.0, and 4.7 V corresponding to ~535 A/cm^2, 660 A/cm^2, and 1150 A/cm^2 current injection for the LEDs with 15%, 8%, and 0% Al in the EBL, respectively. As shown in Fig. 3, the calculated overflow current increases with the applied voltage, and the amount of electron overflow increases with decreasing EBL barrier height. For $V_T=6$ V, the calculated

overflow current percentiles are 68%, 16%, and 2% for the LEDs with 0%Al, 8%Al, and 15% Al in EBLs, respectively. Moreover, and not surprisingly, the percentile overflow for each LED shows a dependence on the applied voltage on the diode: when the voltage increases from 4 to 16 V, the overflow increases from 56% to 80% for the LED with 0% Al in EBL, and from 0% to 42% for that with 15% Al in EBL. It should be reiterated that this calculation is a simplified first order estimation of the electron overflow; we assumed a constant phonon scattering rate regardless of the current. However, as has been reported[17] the phonon lifetime decreases with increasing electron density, which translates to increasing current or the forward bias voltage, causing a decrease in the calculated electron overflow. In other words, our calculations would overestimate the dependence of electron overflow on applied voltage (or current). Second, the effect of electric field inside the active region on the electron velocity has been neglected as well as a simplified band diagram having been used for the calculations. However, even with the simplifying assumptions, a good agreement between the calculations and experiments is obtained. Obviously, these detailed processes would need to be incorporated eventually into the models of the kind under discussion here.

C. Elimination of electron overflow through SEI

Consider a double heterostructure (DH) LED but with an InGaN SEI inserted between the n-GaN layer and the active region ($In_{0.2}Ga_{0.8}N$). The SEI consists of several $In_yGa_{1-y}N$ layers, their In fraction (y) increases in a stepwise manner starting with a low value at the first step near the junction with n-GaN. Since the conduction band discontinuity is small at the first step, the additional kinetic energy and velocity acquired by an injected electron are reduced. As a result, the probability to avoid scattering [Eq. (3)] decreases while the probability to be scattered [Eq. (4)] increases. Therefore, the electrons would be thermalized more efficiently by interacting with LO phonons, and the electron overflow would be decreased or very likely eliminated. In order to quantify the extent of the reduction in the amount of electron overflow or its elimination by employing an InGaN-based SEI, in such a way as to provide energy steps, in one or combination of more than one, equal to or greater than the LO phonon energy, we performed first order calculations of the electron overflow for the LEDs with and without SEI (both without EBL) under different forward voltages across the active region. For simplicity of calculation and also a clearer demonstration, a one-layer SEI (with one intermediate layer of $In_{0.10}Ga_{0.90}N$) was employed (see the inset of Fig. 4). The entire SEI region simulated has a total thickness of 15 nm, which is the same as the total thickness of the three-layer staircase region of the LEDs investigated experimentally. An SEI with higher number of steps, as was done in our experiments, will not change the nature of this discussion.

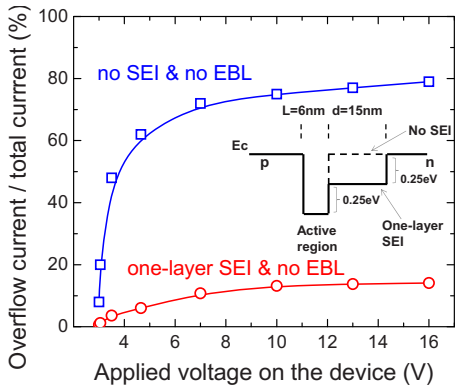

FIG. 4. (Color online) Calculated (overflow electron current/total electron current) as a function of the applied forward voltage across the LED without the SEI and without EBL, and the LED with a 1-layer InGaN SEI and without EBL. Symbols represent the calculated values and solid lines are guides to the eye. The inset shows the simplified conduction band edge for the LEDs with and without (dashed line) the SEI.

The probability of ballistic electron transport across the active region with one-layer SEI is given by

$$P_5 = \frac{\int_{\max[0,(\phi_{EBL}-qV)]}^{+\infty} f(E)N(E)\cdot \exp\{-[d/v_1(E+\Delta E_{c1}) + L/v_2(E+\Delta E_{c2})]/\tau_{sc}\}dE}{\int_0^{+\infty} f(E)N(E)dE}, \quad (9)$$

where $d=15$ nm and $L=6$ nm are the thicknesses of the staircase region ($In_{0.10}Ga_{0.90}N$) and the active region, respectively, and v_1 and v_2 are the electron velocities in the staircase region ($In_{0.10}Ga_{0.90}N$) and the active region, respectively. The energies, ΔE_{c1} ($\sim$0.25 eV in this case) and ΔE_{c2} ($\sim$0.5 eV in this case) represent the excess energy gained by electrons from the conduction band discontinuities upon injection into the $In_{0.10}Ga_{0.90}N$ staircase layer and cascading down to the $In_{0.20}Ga_{0.80}N$ active layer, respectively. For simplicity, we assume that the electrons move in the normal direction to the heterointerfaces. However, this assumption will not have a significant effect on the estimated probability as without this assumption electron thermalization would be enhanced on top of that accorded by the presence of SEI which is very effective to begin with.

In calculating the percentile of the overflow current due to the electrons that experience one scattering event we need to consider four different cases: *only one phonon emission or absorption in the staircase layer or the active region*. As an example, the total probability of electron overflow via "*only one phonon emission in the staircase region*" is composed of the following five components:

(a) Probability of finding an electron conducive for this process (with energy $\hbar\omega_{LO}$ higher than the bottom of conduction band of the n-GaN layer, as an example, for the case of no EBL and flat bands), which is described by P_a in Eq. (2).
(b) Probability to reach x without being scattered, which is described by P_b in Eq. (3), except ΔE_{c1} in place of ΔE_c.
(c) Probability to emit a phonon between x and $x+dx$, which is described by P_c in Eq. (4), except ΔE_{c1} in place of ΔE_c.
(d) Probability to reach $x=d$ without being scattered

$$P_d = \exp\{-[(d-x)/v_1(E+\Delta E_{c1}-\hbar\omega_{LO})]/\tau_{sc}\}, \tag{10}$$

where $v_1(E+\Delta E_{c1}-\hbar\omega_{LO})=\sqrt{2(E+\Delta E_{c1}-\hbar\omega_{LO})/m_e}$.
(e) Probability to reach $x=d+L$ from $x=d$ without being scattered

$$P_e = \exp(-[L/v_2(E+\Delta E_{c2}-\hbar\omega_{LO})]/\tau_{sc}), \tag{11}$$

where $v_2(E+\Delta E_{c2}-\hbar\omega_{LO})=\sqrt{2(E+\Delta E_{c2}-\hbar\omega_{LO})/m_e}$.

Therefore, the probability of just one phonon emission in the staircase region is given by

$$P_6 = \left[\int_0^{+\infty} f(E)N(E)dE\right]^{-1} \int_{\max[0,(\phi_{EBL}-qV+\hbar\omega_{LO})]}^{+\infty} f(E)N(E)\int_0^d \frac{\exp\{-[x/v_1(E+\Delta E_{c1})]/\tau_{sc}\}}{v_1(E+\Delta E_{c1})\cdot\tau_{em}} \times \exp\{-[(d-x)/v_1(E+\Delta E_{c1} - \hbar\omega_{LO}) + L/v_2(E+\Delta E_{c2}-\hbar\omega_{LO})]/\tau_{sc}\}\cdot dx\cdot dE. \tag{12}$$

The probability of only one phonon emission in the active region is given by

$$P_7 = \left[\int_0^{+\infty} f(E)N(E)dE\right]^{-1} \int_{\max[0,(\phi_{EBL}-qV+\hbar\omega_{LO})]}^{+\infty} f(E)N(E)\int_0^d \frac{\exp\{-[d/v_1(E+\Delta E_{c1})]/\tau_{sc}\}}{v_2(E+\Delta E_{c2})\cdot\tau_{em}} \times \exp\{-[(x-d)/v_2(E+\Delta E_{c2}) + (d+L-x)/v_2(E+\Delta E_{c2}-\hbar\omega_{LO})]/\tau_{sc}\}\cdot dx\cdot dE. \tag{13}$$

Similarly, one can obtain the probabilities for one phonon absorption events as well. The extent of the total electron overflow is obtained by summing the electron overflow due to both ballistic electrons (no scattering) and quasiballistic electrons (one scattering event). The contribution to overflow by electrons experiencing two or more scattering events can safely be neglected, as the step in SEI considered here is 0.25 eV below the bottom of the p-GaN conduction band and the electrons thermalized in the SEI (after multiple scattering events) have a very low probability to escape the active region. These multiple scattering events however should be taken into consideration for a more accurate calculation especially for the case of a shallow-step SEI at high injection levels.

Figure 4 shows the calculated percentile overflow electron current, namely the overflow electron current divided by the total current, for two *m*-plane DH LEDs without EBL: one with and another without the SEI structure. The overflow current is 56%–80% of the total current within the range of applied voltages of 4 to 16 V for the LED without any SEI, which is approximately three to five times larger than that of the LED with a one-layer InGaN SEI. It should be noted that for the flat band case, the electron overflow percentile is reduced to 8% with the inclusion of the particular SEI, which is still smaller than that (18%-not shown) for an LED with an increased active layer thickness, 6+15 nm, but without any SEI (i.e., SEI step chosen to be 0.5 eV below the bottom of the p-GaN conduction band). These results suggest that for the one intermediate layer SEI case, a sufficiently large step height and a larger SEI thickness will reduce the electron overflow substantially if not totally eliminate it. An optimum step height for the SEI would provide a balance between the gained electron kinetic energy in the staircase region and the overflow contribution from the electrons thermalized within the SEI.

It should be pointed out that more layers in the SEI (with potential steps no less than one LO phonon energy), like in our experiments (3-layer SEI), might provide additional freedom in the design of such structures and result in smaller electron overflow percentile. However, growth related issues in terms of the effect of SEI on the material quality and strain inside the active region[19,20] should also be taken into consideration when optimizing the SEI layer stack for maximizing the LED efficiency.

D. Effect of polarization on electron overflow

Since the majority of commercial InGaN LEDs are grown on the polar *c*-plane orientation, the polarization field must be incorporated into the above-described theoretical model to be representative of the vast majority of LEDs produced and reported. In order to calculate the electron overflow in *c*-plane LEDs, it is necessary to consider the polarization field-induced band bending in the InGaN active region and EBL to obtain the potential energy differences of the conduction bands of n-GaN (where the electrons are injected) and EBL under various bias conditions. Again, we accomplished this task with the aid of the SILVACO ATLAS commercial software package; however, it should be pointed out that these band structure calculations consider equilib-

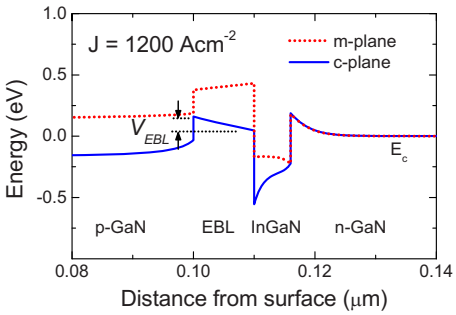

FIG. 5. (Color online) Calculated conduction band edge of *c*-plane (solid line) and *m*-plane (dotted line) InGaN LEDs with a 6 nm $In_{0.15}Ga_{0.85}N$ active region and a 10 nm $Al_{0.15}Ga_{0.85}N$ EBL. The injection current density for both LEDs is 1200 A cm^{-2}.

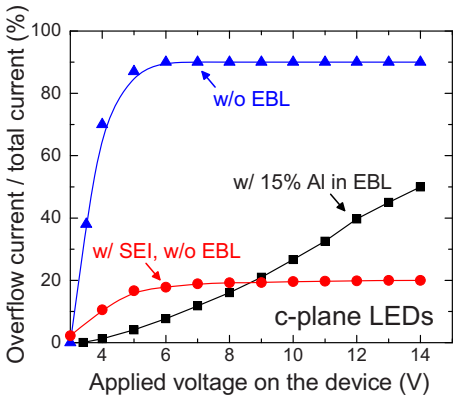

FIG. 6. (Color online) Calculated electron overflow current as a function of the voltage applied across the device for *c*-plane DH LEDs (6 nm $In_{0.15}Ga_{0.85}N$ active region) with different EBL heights (i.e., y=0% Al and 15% Al in $Al_yGa_{(1-y)}N$) and without SEI as well as a *c*-plane DH LED with SEI and without any EBL. Any voltage drop across metal/semiconductor contacts is neglected.

rium carriers only and the hot carriers considered here for understanding electron overflow are not taken into account. For the simulations, polarization charge densities of 4×10^{12} cm^{-2} and 1×10^{13} cm^{-2} have been used for the InGaN active region and the EBL with 15% Al, respectively, which are 60% of the theoretical prediction,[1] in order to facilitate the numerical convergence of SILVACO ATLAS. The other parameters are the same as those enumerated in Sec. II A. Figure 5 shows the simulated conduction band edge profile for a *c*-plane DH LED with a 6 nm active region and 15% Al in EBL, along with the *m*-plane counterpart under the same injection current for comparison. Due to the polarization induced field in the AlGaN EBL as well as the InGaN active region in the *c*-plane case, the conduction bandedge of EBL is "pulled down" at the active region side (due to the immobile positive polarization charge at the active region/EBL interface) even at the 1200 A cm^{-2} current density. It is for the time being assumed that the thermionic emission is the mechanism for the electrons (those that have traversed the active region by ballistic or quasiballistic transport) to surpass the EBL, which has a probability proportional to $\exp(-V_{EBL}/kT)$, where V_{EBL} is the potential drop in the EBL (see Fig. 5). The total electron overflow percentile is obtained by the product of the probability for electrons traversing the active region and the thermionic emission term $\exp(-V_{EBL}/kT)$. It should also be noted that when compared to its *m*-plane counterpart (dotted line), the polarization field in the *c*-plane LED (solid line) reduces the effective barrier of the EBL for the electrons that have traversed the active region,[11] which suggests a higher probability for electrons to escape the active region in the *c*-plane LEDs. Therefore, an approach such as the incorporation of SEI would be needed even more in the *c*-plane LEDs so to cause efficient electron thermalization.

The calculated percentile of electron overflow for *c*-plane 6 nm DH LEDs is shown in Fig. 6. In the case where no SEI is employed, the LED without EBL (solid circles) in overall shows a much higher electron overflow percentile than the one with 15% Al in the EBL (solid squares). Moreover, the overflow in the LED without an EBL saturates at 90% once the applied voltage exceeds 5 V, while for the LED with 15% Al in EBL the overflow increases with the applied voltage: from 0% to 50% when the voltage increases from 3 to 14 V. For the *c*-plane LED which has a one-layer SEI and no EBL, the calculated electron overflow is greatly reduced (~4.5 times lower which is consistent with experiments as will soon be shown) compared to that having no SEI and no EBL. Just for reference, the simulated current densities corresponding to 5 and 14 V externally applied bias (neglecting any voltage drop across metal/semiconductor contacts) are ~990–1000 A cm^{-2} and ~6820–6850 A cm^{-2}, respectively, for all three LEDs. Also at 5 and 14 V applied bias, the net potential drop across the InGaN active region is, respectively, ~0.11 V and ~0.05 V for the *c*-plane LED with an $Al_{0.15}Ga_{0.85}N$ EBL, ~0.33 V and ~0.25 V for the *c*-plane LED without any EBL, and ~0.08 V and ~0.002 V for the *c*-plane LED with one-layer SEI.

It is evident that the *c*-plane LEDs (Fig. 6) have higher electron overflow than their *m*-plane counterparts (Fig. 3) having the same structures. This is due to the polarization induced band bending in the InGaN active and EBL regions of the *c*-plane LEDs which results in a reduced effective barrier provided by EBL (Fig. 5). In this regard, the polarization field exacerbates the electron overflow in LEDs. Again, the responsible mechanism behind the electron overflow is the ballistic and quasiballistic electron transport since the EL efficiency loss caused by electron overflow is also present in the *m*-plane LEDs, which is free of polarization induced field. We should note that the calculations do not take into consideration the effect of acceleration of electrons under the electrical field within the active region, when band bending exists, which might have underestimated the calculated percentiles of overflow. It is worth mentioning that in the current *c*-plane case even without considering the acceleration of the electron by the electric field, the probability for an electron to traverse the active region and reach the EBL (before surpassing the EBL) is already ~90% (in both 0% Al and 15% Al EBL cases) due to the lowering of the barrier in the p-region by the polarization induced electric filed. Marginal (3%–5%) enhancement of the ballistic or quasiballistic electron transport is gained by adding the electric field acceleration effect on the electron velocity in the present case.

III. EXPERIMENTAL RESULTS

The investigated *m*-plane LED structures were grown on freestanding *m*-plane $(1\bar{1}00)$ GaN substrates in a vertical low-pressure metalorganic chemical vapor deposition system. The ~500 μm-thick *m*-plane freestanding GaN substrates, produced at Kyma Technologies, Inc., had a threading dislocation density of $<5\times10^6$ cm^{-2} and were off-cut by 0.2° toward the GaN *a*-axis and 0.3° toward the GaN *c*-axis. The LED structures contain a 6 nm undoped active region of $In_{0.20}Ga_{0.80}N$ ($\lambda_{peak}\sim440$ nm) followed by a 3 nm undoped $In_{0.01}Ga_{0.99}N$ layer. Just beneath the 6 nm active layer, a 60 nm Si-doped (2×10^{18} cm^{-3}) $In_{0.01}Ga_{0.99}N$ underlayer was employed for improved active region quality unless otherwise specified. A ~10 nm EBL of *p*-$Al_xGa_{1-x}N$ (x=15%, or 8%, or 0%) was deposited on top of the active layer. The final Mg-doped p-GaN layer was about 100 nm thick with a nominal hole density of 7×10^{17} cm^{-3}. The *c*-plane DH LEDs investigated in the present work were grown on *c*-plane sapphire substrates with *in situ* SiN_x nanonetwork,[21] and have a 6 nm $In_{0.15}Ga_{0.85}N$ active region with a peak emission wavelength of ~410 nm. The structures of the *c*-plane LEDs are the same as their *m*-plane counterparts, except for the In composition (i.e., emission wavelength) of the active layer. After mesa (250 μm diameter) formation, Ti/Al/Ni/Au (30/100/40/50 nm) metallization annealed at 800 °C for 60 s was used for *n*-type Ohmic contacts, and 5 nm/5 nm Ni/Au semitransparent p-contacts were employed. Finally, 50 μm diameter 30/50 nm Ni/Au contact pads were deposited on part of the mesa tops for the on-wafer probed EL measurements.

The internal quantum efficiency (IQE) was extracted from the excitation power-dependent PL[13,22] measurements at room temperature using a frequency-doubled 80 MHz repetition rate femtosecond Ti:sapphire laser. The excitation wavelength was 370 nm, below the band gap of the barriers and the top GaN layer. As such, the photoexcited electron-hole pairs were generated only in the InGaN active layer, which circumvents optical carrier generation in the barriers and also electrical carrier injection related ailments which cause efficiency degradation in the EL case.[11,23] On-wafer EL measurements were performed using pulsed current (1 μs pulse width, 0.1% duty cycle) without any special means to enhance light extraction. While the light collection geometry was kept the same among all the measurements, no attempt was made to capture all of the photons emitted by the LEDs tested.

A. EL efficiency of InGaN LEDs without SEI

Figure 7(a) shows the relative EQE as a function of the current density for the *m*-plane LEDs with different Al composition in their EBLs, the structures of which are described above. In general, the EQE decreases as the Al mole fraction in the EBL is reduced. According to our resonant PL measurements described above, the three LED structures have essentially the same IQE for the same injected carrier density (IQE of 50%–56% at a carrier density of 1×10^{18} cm^{-3} under the assumption that the radiative recombination coefficient B is 1×10^{-11} cm^3 s^{-1}). It is, therefore, reasonable to

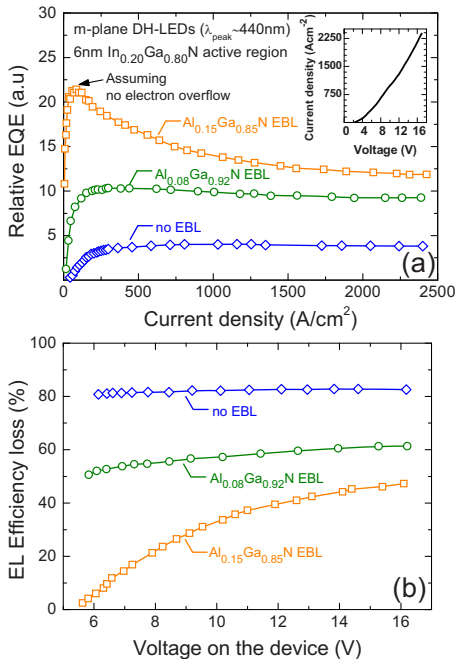

FIG. 7. (Color online) (a)Relative EQE of *m*-plane LEDs grown on freestanding *m*-plane $(1\bar{1}00)$ GaN substrates with varying Al composition (15%, 8%, and 0%) in the EBL layers, measured under pulsed current, 1 μs pulse width and 0.1% duty cycle. The inset shows the current-voltage dependence for the LED with 15% Al in EBL. (b) The EL efficiency loss as a function of the external applied voltage across the p-n junction of the LEDs, assuming negligible electron overflow at the current density (~80 A cm^{-2}) corresponding to the peak efficiency for the LED with 15% Al in EBL, which is very reasonable according to our calculations.

suggest that the different EL efficiencies for LEDs with varying EBLs originate from carrier injection and more likely carrier overflow rather than the quality variation among the active regions. The EQE for the *m*-plane LED with 15% Al in EBL (open squares in the figure) peaks at approximately 85 A cm^{-2}, and the efficiency drops by ~45% with increasing current injection up to 2400 A cm^{-2}. A negligible efficiency drop (~3–5%) is observed for the structure without an EBL (i.e., for 0% Al in EBL) with increasing injection. Another observation is that its relative EQE (Fig. 7) is approximately three to five times lower than that with 15% Al in the EBL. Intermediate values for EQE and efficiency drop (~10%) are obtained for the LED with 8% Al within EBL (Fig. 7).

If we assume that the LED with EBL having 15% Al has negligible electron overflow at a current density of 80 A cm^{-2} and also the relatively low EL efficiency at current densities before reaching the peak efficiency for each LED is due to SRH recombination, we can then obtain the efficiency loss due to electron overflow according to the results in Fig. 7(a). Figure 7(b) shows the percentile EL efficiency loss due to the electron overflow as a function of the applied voltage across the LEDs (including the voltage drop across the contacts). In the LED without the EBL, 20% of the overall current contributes to the EL and approximately 80% of the current is due to electrons traversing the active region without contributing to the light emission. As we mentioned above, the voltage drop across the active region reduces the effective barrier by the p-side for the electrons,

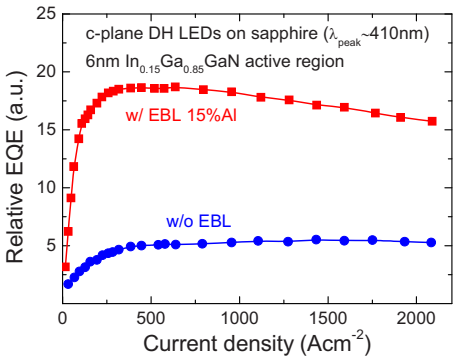

FIG. 8. (Color online) Relative EQE of *c*-plane DH LEDs grown on *c*-plane GaN templates on sapphire with and without an EBL layer. The LEDs were measured under pulsed current, 1 μs pulse width and 0.1% duty cycle.

and therefore, results in increased electron overflow with increasing applied voltage. In the LED with 15% Al in the EBL, the efficiency loss at 16 V is ~45%, which means that ~45% of the injected electrons are the overflow electrons since we have assumed, reasonably so, that this LED has negligible electron overflow at current densities at or below 80 A cm^{-2}. The results are in good overall agreement with the theoretical estimations [Fig. 3(b)]: the increase in the overflow current component with decreasing EBL barrier height and its weaker dependence on the applied bias for lower EBL barrier heights are both predicted by our theory and consistent with our experiments. A more accurate estimation of the loss of the EL efficiency needs to take into account the dependence of IQE on the injected carrier concentration, electron and hole wave function overlap inside the active region, and phonon lifetime dependence on the electron density, etc.

It should be noted that the polarization induced electric field in the *c*-plane InGaN active region and the EBL has also been proposed to be the reason for the electron overflow to the *p*-GaN layer.[11] In this regard, we studied the *c*-plane LEDs as well to investigate the correlation between the polarization field and LED EL efficiency. Figure 8 shows the relative EQE data for two *c*-plane DH LEDs: one with a 10 nm $Al_{0.15}Ga_{0.85}N$ EBL and one without any EBL. The LED with EBL exhibits three to four times higher EL intensity than that without any EBL. This indicates that as in the case of *m*-plane LEDs, the absence of EBL has resulted in a comparable degree of loss in the EL efficiency which can be attributed to increased electron overflow in the case without EBL.

B. EL efficiency of InGaN LEDs with SEI

In order to test our premise in regard to hot electrons and the ensuing ballistic and quasiballistic electron transit across the active region without partaking in the recombination process, (without complete thermalization and reaching equilibrium with the lattice), two *m*-plane LEDs, to be followed by the *c*-plane counterparts, were investigated [see Fig. 9(a) for the device schematics]: one LED with a 10 nm *p*-AlGaN EBL with 15% Al, while the other without any EBL at the *p*-region, and both having a SEI under the InGaN active region to cause the thermalization of the injected electrons.

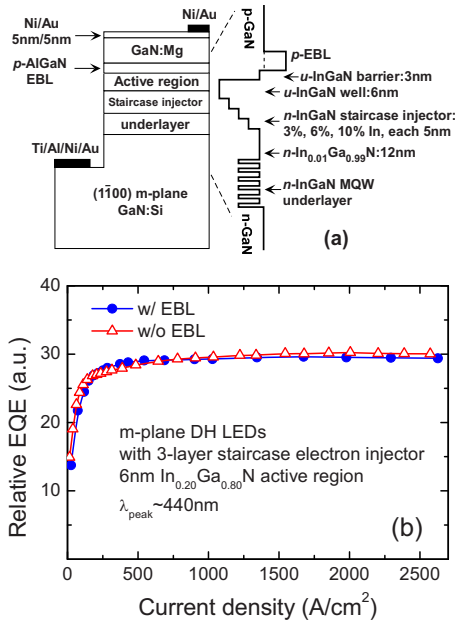

FIG. 9. (Color online) (a) Schematic for the two *m*-plane LEDs with InGaN SEI before the active regions (to thermalize the injected electrons from the n-GaN layers), one of which has a 10 nm EBL with 15% Al and the other one without any EBL in the *p*-region. (b) Relative EQE of the two *m*-plane LEDs with SEI: one with and one without EBL. The LEDs were measured under pulsed current, 1 μs pulse width and 0.1% duty cycle.

As will be seen below, we extended this study to include the *c*-plane variety as well. The SEI consists of three 5 nm InGaN layers with In compositions of 3%, 6%, and 10%, in order starting from the n-GaN side, as shown in Fig. 9(a) (the first step height going from n-$In_{0.01}GaN$ to the first SEI layer, $In_{0.03}GaN$, is very close to or smaller than an LO phonon energy (88 meV); therefore, the first two SEI layers may be considered as a single step for electron cooling via LO phonon emissions. The step heights for other steps in the SEI are more than the LO phonon energy as desired.). In order to circumvent the quality degradation by the SEI layer, a six-period $In_{0.01}Ga_{0.99}N(7\ nm)/In_{0.06}Ga_{0.94}N(3\ nm)$ multiple quantum well (MQW) underlayer was employed prior to the active layer underneath the 12 nm thick $In_{0.01}Ga_{0.99}N$ layer and the InGaN SEI to improve the active region quality. The underlayer and the SEI were *n*-type doped with Si to an electron density of 2×10^{18} cm^{-3}. Figure 9(b) shows the relative EQE of the two *m*-plane LEDs with SEI. The results confirm that the LED with EBL has essentially the same EL intensity (i.e., relative EQE) as the one without EBL. This is substantially different from what we have observed in Fig. 7(a) in regard to devices not featuring a SEI, where the EL intensity from the LED without EBL is three to five times lower than the one with EBL. It is, therefore, reasonable to suggest convincingly that by employing the InGaN SEI before the active region, the electron overflow due to ballistic or quasiballistic electron transport across the active region is eliminated, which has resulted in a similar EL performance for the two LEDs with SEI regardless of the EBL status. This is reasonable considering that the electron overflow solely due to thermionic emission is negligible (even for the LED without EBL) according to the discussion in Sec. II A.

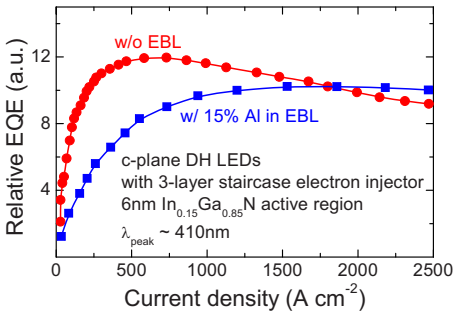

FIG. 10. (Color online) Relative EQE of two *c*-plane LEDs with SEI inserted under the active region: one with and one without EBLs. The LEDs were measured under pulsed current with 1 μs pulse width and 0.1% duty cycle. The SEI includes three intermediate InGaN layers with In compositions of 3%, 6%, and 10%, in the given order.

Similar to the *m*-plane case, the significant difference between the LEDs with an EBL and without EBL is eliminated when an InGaN-based SEI structure is employed in the *c*-plane LED case as well. The same three-ayer SEI and the MQW underlayer (for improving the active region materials quality) structures used in *m*-plane LEDs are employed also for the *c*-plane LEDs. Both *c*-plane LEDs with SEI under investigation, one with EBL (15% Al) and the other without any EBL, exhibit essentially the same IQE as determined from optical measurements with resonant excitation (IQE of 46%–50% at a carrier density of 1×10^{18} cm^{-3} assuming a radiative recombination coefficient B of 1×10^{-11} cm^3 s^{-1}). Figure 10 shows that when the SEI is employed, the difference in relative EQE between the LEDs with and without EBL is significantly reduced as compared to that in LEDs without SEI in Fig. 8. This once again suggests that by using the SEI the ballistic and quasiballistic electron transport across the active region is substantially reduced. Moreover, the injection current dependence of the efficiency in the *c*-plane LEDs with SEI deviates somewhat from that of the *m*-plane LEDs with SEI, where essentially the same EQE values were observed for the LEDs with and without EBL for all injection current levels. Somewhat unexpectedly, in the *c*-plane case the LED without EBL shows even higher EQE than that with the EBL when the current density is below 1700 A cm^{-2}. At low current densities ($<$500 A cm^{-2}), the EQE from the LED without EBL is 1.7–2.5 times higher than the one with EBL. When the current density is above 1700 A cm^{-2}, the former shows slightly lower EQE values than the latter ($<$8%), within nominal variations due to, e.g., processes such as current filamentation. The removal of the EBL has a more significant improvement in terms of EQE for the *c*-plane LEDs than for the *m*-plane ones, which might result from a more inferior hole transport across the EBL in the *c*-plane case due to relatively larger hole effective mass compared to that in the *m*-plane LEDs and or relatively lower hole concentrations. Additionally, the 22% efficiency degradation observed for the LED with SEI and without EBL when the current density is increased up to 2500 A cm^{-2} might suggest that the *c*-plane orientation requires more thermalization due to its polarization field in order to avoid the electron overflow-induced EL efficiency loss. This is of course assuming that processes such as current filamentation are not in play here.

IV. DISCUSSION

In both *m*-plane (nonpolar) and *c*-plane (polar) LEDs, the EBL affects the LED EL performance substantially: the LEDs without any EBL show three to five times lower EL intensity (EQE as well) as compared to the LEDs with an $Al_{0.15}Ga_{0.85}N$ EBL (see Figs. 7 and 8). Naturally, the height of the barrier, determined by the AlN molar fraction used, affects the EL efficiency as well (see Fig. 7). In aggregate, therefore, the data suggest that the electron overflow is very likely a major contributor, if not the only contributor, to the efficiency loss at high injection current levels. As mentioned in Sec. II A the electron overflow due to the thermionic emission of the equilibrium electrons inside the active region is very negligible even at an artificially high junction temperature of 1000 K. This means that thermionic emission is not the genesis of electron overflow, and further the electron overflow process under discussion can be constructed as temperature independent within the realm of practical junction temperatures. It is, therefore, very reasonable to consider that the electron overflow is caused by nonequilibrium electrons (i.e., the ballistic and quasiballistic electrons). In this realm (as illustrated in Fig. 2), the electrons gain kinetic energy once injected to the active region which equals to the conduction band discontinuity (ΔE_c) between the n-GaN layer (injector) and the InGaN layer (active region). As supported by the agreement between our nonequilibrium-electron-based theory and experiments, the majority of these hot electrons in the structures considered traverse the active region to a large extent and contribute to the overflow current without contributing to any recombination process, thereby reducing the LED EL efficiency. The electron overflow percentiles calculated with our first order model (Fig. 3 for the *m*-plane case, Fig. 6 for the *c*-plane case) indicate that the electron overflow strongly depends on the barrier height of EBL and also the applied voltage across the junction, which is consistent with our experimental data. It should be reiterated that in our first-order calculations, for simplicity and also a more clearer demonstration, we assumed a constant phonon scattering rate regardless of the current (hence the carrier concentration inside the active region). Furthermore, the effect of electric field inside the active region on the electron velocity has been neglected as well as a simplified conduction band edge diagram having been used for the calculations.

Armed with the knowledge of ballistic and quasiballistic transport, the efficiency degradation caused by the hot electrons can either be reduced by an EBL (to block the escaping electrons) or a SEI (to thermalize the hot electrons before they are injected into the active region). However, the EBL not only acts to reduce electron overflow, but also presents a barrier for hole injection, albeit a relatively small one, which is not desirable considering that hole injection is already hampered due to relatively low hole density on the p-side. Moreover, in the *c*-plane LED case (the most commonly used orientation), the polarization field inside the active region and EBL could greatly reduce the effective barrier of

the EBL for the electrons.[24] The employment of a SEI automatically reduces the gained kinetic energy of the injected electrons by reducing the conduction band discontinuity to about one LO phonon energy or slightly above. This increases the electron transit time during which the hot electrons would be more likely thermalized by LO phonon scattering, not to mention the barrier they will face on the other side of the active region, which culminates into reducing the electron overflow. This picture is supported by our theoretical calculations [Fig. 4 for *m*-plane case, Fig. 6 for *c*-plane case)]. Once the injected electrons are thermalized, the need for EBL is more or less eliminated.

Considering the experimental data for LEDs featuring the SEI once again, it is clear that essentially the same EL performance exhibited by the *m*-plane DH LEDs with and without EBL (Fig. 9) is consistent with the above model, namely the overflow is caused by the ballistic and quasiballistic electrons. The incorporation of a SEI eliminates the ballistic and quasiballistic electrons in the LED active region. Whether an EBL is employed in the SEI LED or not makes no discernable difference in terms of the electron overflow (therefore the EL efficiency) due to negligible thermionic emission of now thermalized (equilibrium) electrons from the active region. In the *c*-plane DH LED case, when a SEI is inserted, the difference of the LEDs with and without EBL is greatly reduced (Fig. 10). Moreover, the *c*-plane LED with EBL even shows lower EL efficiency than the one without EBL when current density is less than 1700 A cm^{-2} (beyond which former shows slightly lower than the latter by a few percent), which is likely due to the impeded hole injection caused by the EBL. This suggests that removal of the EBL in favor of the SEI is beneficial to the performance of *c*-plane LEDs as well.

The concept of the reduction in EL efficiency due to the ballistic and quasiballistic electrons and the elimination of these hot electrons by the employment of a SEI structure should apply to the design of both InGaN LEDs and laser diodes. For the latter case where the threshold current densities as high as a few kiloampere per square centimeter are generally used, the carrier thermalization and capture processes become an even more critical issue. We should also point out that our first order simplified theory, even with its limitations, predicts the salient features of experimental observations in aggregate which heretofore has been lacking. Consideration of the electron density dependent LO phonon lifetimes, which reduce with increasing electron density for the concentrations in effect here, would enhance the accuracy. The same is also applicable for not limiting the direction of motion before and after the scattering events. Furthermore, accurate models taking into account more accurate band edge profiles in the presence of carrier injection, and consideration of electron velocity with respect to electric field would enhance the model. Clearly, impetus is in place for the assumptions made in our first order theory to be replaced with a more accurate treatment. Again, we would like to underscore that consideration of hot electrons, and their ballistic and quasiballistic transport across the active region is revolutionary when it comes to light emitters such as those discussed here. In such a framework, there is a very good agreement between the theory and experiments involving LEDs with polarization void *m*-plane and polar *c*-plane orientations with and without EBL of varying barrier height and with and without SEI.

V. CONCLUSIONS

Using LED structures with varying EBL (0%–15% Al) barriers, we determined the presence of ballistic and or quasiballistic electrons in the active layer and their role in efficiency reduction in general and with increasing current in particular by considering the electron scattering and transport in this new realm. Specifically, we developed first order models utilizing the LO phonon scattering rates to describe the electron overflow to the *p*-type region resulting in three to five times lower EL intensity in LEDs without the EBL compared to those with $Al_{0.15}Ga_{0.85}N$ EBL both for *c*-plane and *m*-plane varieties. For an effective means of thermalization, and therefore, reduction in the ballistic and quasiballistic transport of the injected electrons to reduce the electron overflow responsible for the efficiency degradation in these devices, an InGaN staircase structure (with step-wise increased In composition) was inserted before the active region. The employment of the SEI resulted in essentially the same EL performance for the LEDs with and without EBL for the polarization charge void *m*-plane case. For the polar *c*-plane LED case, up to a factor of 2.5 improvement has been observed in EQE when SEI was inserted but EBL removed for current densities below 1700 A cm^{-2} due possibly to enhanced hole injection since the EBL also impedes the hole transport. The analysis of nonequilibrium carriers and the SEI approach to reduce electron overflow proposed here for LEDs are applicable to GaN-based laser diodes as well. Another underlying perspective that one might glean from the model and data presented is the validity of the commercial and otherwise software codes lacking the nonequilibrium carrier physics that are very commonly used nowadays to predict/model InGaN based LEDs.

ACKNOWLEDGMENTS

The work at VCU is funded by grants from the Air Force Office of Scientific Research (Dr. K. Reinhardt), and the National Science Foundation, and that at the Semiconductor Physics Institute is funded by the Air Force Office of Scientific Research. One of us (A.M.) is grateful to Window of Science program supported by AFMC (ITO–TEL-037).

[1]H. Morkoç, *Handbook of Nitride Semiconductors and Devices* (Wiley-VCH, Weinheim, Germany, 2008), Vol. 3, Chap. 1.
[2]M. R. Krames, O. B. Shchekin, R. Mueller-Mach, G. O. Mueller, L. Zhou, G. Harbers, and M. G. Craford, J. Disp. Technol. **3**, 160 (2007).
[3]Y. C. Shen, G. O. Mueller, S. Watanabe, N. F. Gardner, A. Munkholm, and M. R. Krames, Appl. Phys. Lett. **91**, 141101 (2007).
[4]N. F. Gardner, G. O. Müller, Y. C. Shen, G. Chen, and S. Watanabe, Appl. Phys. Lett. **91**, 243506 (2007).
[5]K. T. Delaney, P. Rinke, and C. G. Van de Walle, Appl. Phys. Lett. **94**, 191109 (2009).
[6]A. R. Beattie and P. T. Landsberg, Proc. R. Soc. London, Ser. A **249**, 16 (1959).
[7]J. Hader, J. V. Moloney, B. Pasenow, S. W. Koch, M. Sabathil, N. Linder, and S. Lutgen, Appl. Phys. Lett. **92**, 261103 (2008).
[8]H. Ryu, H. Kim, and J. Shim, Appl. Phys. Lett. **95**, 081114 (2009).

[9]G. Chen, M. Craven, A. Kim, A. Munkholm, S. Watanabe, M. Camras, W. Götz, and F. Steranka, Phys. Status Solidi A **205**, 1086 (2008).
[10]K. A. Bulashevich and S. Y. Karpov, Phys. Status Solidi C **5**, 2066 (2008).
[11]M. H. Kim, M. F. Schubert, Q. Dai, J. K. Kim, E. F. Schubert, J. Piprek, and Y. Park, Appl. Phys. Lett. **91**, 183507 (2007).
[12]J. Xie, X. Ni, Q. Fan, R. Shimada, Ü. Özgür, and H. Morkoç, Appl. Phys. Lett. **93**, 121107 (2008).
[13]J. Lee, X. Li, X. Ni, Ü. Özgür, H. Morkoç, T. Paskova, G. Mulholland, and K. R. Evans, Appl. Phys. Lett. **95**, 201113 (2009).
[14]X. Ni, Q. Fan, R. Shimada, Ü. Özgür, and H. Morkoç, Appl. Phys. Lett. **93**, 171113 (2008).
[15]Ü. Özgür, H. Liu, X. Li, X. Ni, and H. Morkoç, Proc. IEEE **98**, 1180 (2010).
[16]K. T. Tsen, R. P. Joshi, D. K. Ferry, A. Botchkarev, B. Sverdlov, A. Salvador, and H. Morkoç, Appl. Phys. Lett. **68**, 2990 (1996).
[17]J. Liberis, I. Matulionienė, A. Matulionis, M. Ramonas, and L. F. Eastman, in *Advanced Semiconductor Materials and Devices Research: III-Nitrides and SiC*, edited by H.-Y. Cha (Transworld Research Network, Kerala, India, 2009).
[18]E. Tiras, M. Gunes, N. Balkan, and W. J. Schaff, Phys. Status Solidi B **247**, 189 (2010).
[19]T. Akasaka, H. Gotoh, T. Saito, and T. Makimoto, Appl. Phys. Lett. **85**, 3089 (2004).
[20]C. Huang, T. Liu, Y. Lu, W. Shiao, Y. Chen, J. Wang, C. Lu, and C. C. Yang, J. Appl. Phys. **104**, 123106 (2008).
[21]J. Xie, Ü. Özgür, Y. Fu, X. Ni, H. Morkoç, C. K. Inoki, T. S. Kuan, J. V. Foreman, and H. O. Everitt, Appl. Phys. Lett. **90**, 041107 (2007).
[22]Q. Dai, M. F. Schubert, M. H. Kim, J. K. Kim, E. F. Schubert, D. D. Koleske, M. H. Crawford, S. R. Lee, A. J. Fischer, G. Thaler, and M. A. Banas, Appl. Phys. Lett. **94**, 111109 (2009).
[23]M. J. Galtrey, R. A. Oliver, M. J. Kappers, C. J. Humphreys, D. J. Stokes, P. H. Clifton, and A. Cerezo, Appl. Phys. Lett. **90**, 061903 (2007).
[24]S. Yen, M. Tsai, M. Tsai, Y. Shen, T. Hsu, and Y. Kuo, IEEE Photon. Technol. Lett. **21**, 975 (2009).